

Operation of bolometer system using Pt foil on SiN substrate detector for EAST tokamak


Y. M. Duan, S. T. Mao, L. Q. Hu, P. Xu, L. Q. Xu, J. Z. Zhang, and S. Y. Lin

Citation: [Review of Scientific Instruments](#) **87**, 11D434 (2016); doi: 10.1063/1.4961268

View online: <http://dx.doi.org/10.1063/1.4961268>

View Table of Contents: <http://aip.scitation.org/toc/rsi/87/11>

Published by the [American Institute of Physics](#)



Small Conferences. BIG Ideas.

Applied Physics
Reviews

SAVE THE DATE!
3D Bioprinting: Physical and Chemical Processes
May 2–3, 2017 • Winston Salem, NC, USA

The background of the banner features a blue-toned image of a human hand holding a glowing, branching structure that resembles a biological or chemical process, possibly a 3D printed model or a biological specimen.

Operation of bolometer system using Pt foil on SiN substrate detector for EAST tokamak

Y. M. Duan, S. T. Mao, L. Q. Hu,^{a)} P. Xu, L. Q. Xu, J. Z. Zhang, and S. Y. Lin
Institute of Plasma Physics, Chinese Academy of Sciences, P.O. Box 1126, Hefei 230031, China

(Presented 6 June 2016; received 3 June 2016; accepted 26 July 2016;
 published online 29 August 2016)

The foil resistive bolometer diagnostic on experimental advanced superconducting tokamak has been upgraded partly with a new generation of detectors. The new detectors have faster response time. However, the microwave interference is still a serious issue for the bolometer system. The system response to microwave is tested, and the test results show that the closed Wheatstone bridge circuit in the detector is the most sensitive component to high power microwave field. Simulation results of microwave transmission by the high frequency structure simulator software and shielding design are also presented. *Published by AIP Publishing.* [<http://dx.doi.org/10.1063/1.4961268>]

I. INTRODUCTION

Bolometer diagnostics are commonly used to measure the plasma total radiated power and the radiation emission profile in many fusion devices.¹⁻³ At present, the metal foil resistive bolometer and the absolute extreme ultraviolet (AXUV) photodiodes are two kinds of typical bolometer detectors. However, the AXUV photodiodes as absolute bolometers are not ideal due to their response deficiency for low energy photons. The foil resistive bolometer is chosen as one of the candidate bolometer detectors for ITER with a high neutron flux radiation condition.⁴⁻⁶

The metal foil resistive bolometer system has been implemented on the Experimental Advanced Superconducting Tokamak (EAST) for several years.⁷ Recently, the bolometer system was upgraded and part of the original detectors were replaced by a new generation of detectors. However, the resistive bolometer system has suffered from the effects of radio frequency (RF) waves at 2.45 GHz and 4.6 GHz which are used as auxiliary plasma heating. In Secs. II-V, a brief description of the bolometer system after upgrade is given in Sec. II. A testing experiment of microwave interference on the bolometer system is introduced in Sec. III. Simulation of microwave transmission by the High Frequency Structure Simulator (HFSS) software and shielding design are reported in Sec. IV. Finally, a brief summary is given in Sec. V.

II. UPGRADE OF THE BOLOMETER SYSTEM

A metal foil resistive bolometer detector generally uses a thin metal foil as an absorber and two interwoven meanders on its back side as measuring resistors. The absorber foil receives plasma radiation and then induces the meander resistances change by heat transfer. The two measurement resis-

tors and another two reference resistors consist of a classical Wheatstone bridge circuit. So, the output of the detector is the unbalanced voltage of the bridge circuit. The EAST bolometer detectors are based on 4 μm thick Pt absorbers deposited on 1.5 μm thick SiN membranes, which is similar to the prototype developed for the ITER bolometer.^{4,6}

The resistive bolometer system on EAST consists of 3 cameras with a total of 48 channels. The spatial resolution, δr , is about 3–4 cm.⁷ The detector shielding structure in the vacuum vessel is upgraded for better enclosing and isolation, which is installed in the horizontal diagnostic port-O, the adjacent port of the low hybrid wave (LHW) antenna, as shown in Fig. 1. The radio frequency (RF) auxiliary heating system on EAST includes three subsystems: a low hybrid wave (LHW) system at 2.45 GHz and 4.6 GHz, an ion cyclotron radio frequency (ICRF) system at 27 MHz, and an electron cyclotron resonance heating (ECRH) system at 140 GHz. An arc-shaped shutter plate is added for aperture protection during wall coating. The water cooling structure is changed from an outer cooling plate to an embedded cooling module, as shown in Fig. 2. In addition, the Data Acquisition (DAQ) system is also optimized to enhance its stability.

With the improvement of processing techniques, part of the original detectors are replaced by a new generation of detectors which have faster response time and lower sensitivity. Fig. 3 shows the calibration results of detector parameters by an electric calibration method.⁸ The calibration is separately carried out in air and in vacuum. It is shown that the sensitivity of the new detectors is much lower than that of the old detectors in both conditions and the cooling time, τ , of the new detectors is also lower than that of the old detectors in the air condition. However, the values of the cooling time, τ , for the new detectors and the old ones are roughly equal in the vacuum condition. The response time of the detector depends on the substrate material and its connection with the absorber foil.⁵ The fast response time of the new detectors is also verified from the measurement signals, shown in Fig. 4. Three channel signals for viewing the same plasma region are compared. The new foil resistive bolometer detector, as well as the AXUV detector,⁹ can respond to fast radiation events

Note: Contributed paper, published as part of the Proceedings of the 21st Topical Conference on High-Temperature Plasma Diagnostics, Madison, Wisconsin, USA, June 2016.

^{a)}Author to whom correspondence should be addressed. Electronic mail: lqhu@ipp.ac.cn.

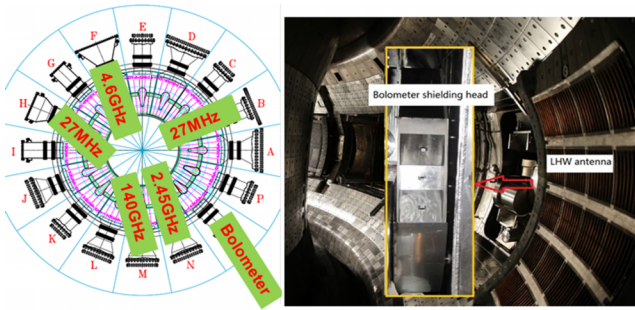


FIG. 1. Bolometer shielding box in vacuum vessel (right) and installation position (left).

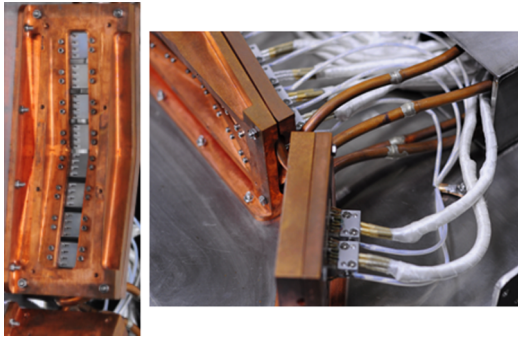


FIG. 2. Detector supporting module with water cooling.

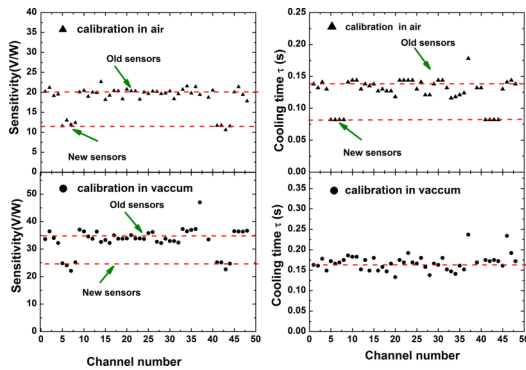


FIG. 3. Calibration results of cooling time τ and sensitivity of detectors.

caused by impurity bursts, but the old foil resistive bolometer detector cannot measure the fast radiation process.

III. MICROWAVE INTERFERENCE TEST

The RF wave auxiliary heating system on EAST includes several different subsystems with frequencies from MHz to GHz. It has been observed in some other tokomaks that the 140 GHz ECRH mm wave easily affects the bolometer detector due to its broad-band sensitive range.^{10–12} At present, no influence from ECRH waves is found on EAST, but the signals have suffered serious interference from LHW waves at 2.45 GHz and 4.6 GHz. A worse signal distortion occurred at the moments of wave injection. The reason is confusing. So, the microwave influences to the bolometer system are tested in a special microwave platform located in the EMC laboratory of the State Grid Electric Power Research Institute.

Fig. 5 shows the microwave test arrangement. The microwave antenna can produce monofrequency waves at 2.45 GHz

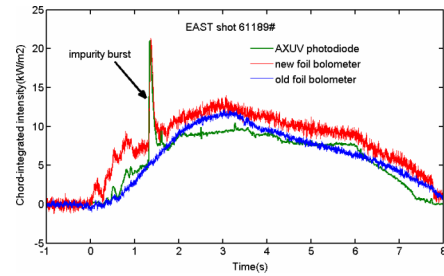


FIG. 4. Signal evolution of different detectors.

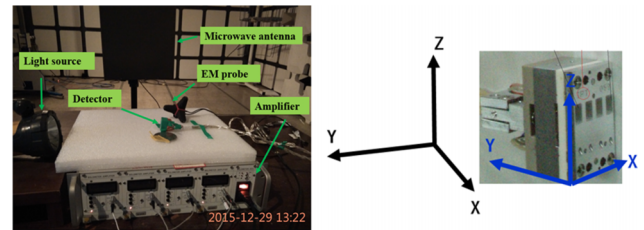


FIG. 5. Photo of microwave test arrangement.

and 4.6 GHz. The propagation direction of the wave along the X axis and the vibration direction of the wave can be adjusted along the Z axis or Y axis. The bolometer system components including detector, amplifier, and cable are placed in the microwave field. A flashlight is used as a light source. The differential output voltages of the amplifier are displayed in the oscilloscope as V_{out+} and V_{out-} . The electric field, E, near the detector is measured by an electromagnetic (EM) probe. The maximum E (250 V/m) is near to the microwave E field measured in the EAST device hall, which is at least two times smaller than the estimated value in the vacuum vessel. The testing results show that the electrical amplifiers have good performance to withstand the interference of the microwave. The detector is the most sensitive component to microwaves. The amplifier output signals at a gain of 1000 are shown in Fig. 6. A modulated flashlight source is used in the cases of Figs. 6(a) and 6(b) and no light source is used in the cases of Figs. 6(c) and 6(d). The signal distortions are captured in both conditions when the microwaves are switched on. There are two kinds of distortions: (1) The signals V_{out+} and V_{out-} roll over to the opposite direction, as shown in Figs. 6(a) and 6(c); (2) the signals V_{out+} and V_{out-} rise sharply in the same direction as shown in Figs. 6(b) and 6(d). That is to say, one signal distortion causes a positive voltage drift and the other distortion causes a negative voltage drift. The phenomenon is consistent with experimental observations. An output voltage drift about ± 4 V is measured in the condition with maximum testing E field, which is about two orders larger than the noise magnitude. In fact, the serious voltage drift caused by the waves during the EAST experiment can reach the saturation value ± 10 V with the same amplifier gain. On the contrary, it is indicated that the wave E field near the bolometer detectors in the EAST vacuum vessel is two times larger than that in the test.

The distortion is also related with the vibration direction of the wave. For 4.6 GHz microwaves, no influence on the detector is observed when wave vibration direction is along the Z axis. For 2.45 GHz microwave, the influences are obvious under the two wave vibration directions. The interference

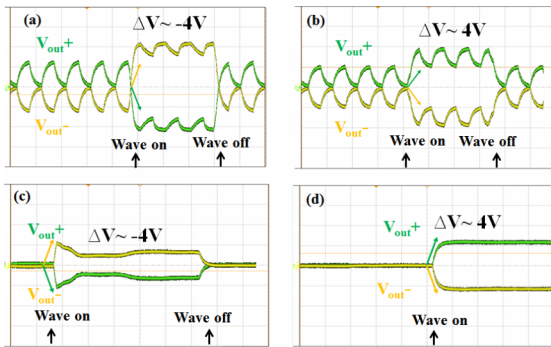


FIG. 6. Amplifier output signals in microwave field. (a) and (b) with modulated flashlight source; (c) and (d) without light source.

intensity is larger when the detector side is perpendicular to the X axis (as Fig. 5 shown) than that when the detector front is perpendicular to the X axis. This phenomenon illustrates that the closed Wheatstone bridge circuit in the detector is affected rather than the absorber foil. It is possible that an induced current is produced in the bridge circuit which can result in a large output voltage drift.

IV. SIMULATION OF MICROWAVE TRANSMISSION AND SHIELDING DESIGN

According to the microwave test results mentioned-above, good shielding for sensors is valid. In fact, there is a collimator aperture in front of the detector shielding box and some other junction gaps which possibly provide coupled paths for microwaves. The performance of microwave transmission through slits is studied using the simulation software HFSS (High Frequency Structure Simulator).

The simplified model of a bolometer detector shielding box in the vacuum vessel is built in the software HFSS platform. The actual size of the bolometer shielding box is reconstructed and a larger square chamber is built as the simulated EAST vacuum vessel. Microwaves with 100 kW power at 2.45 GHz and 4.6 GHz are injected from a front port. The vacuum chamber is large enough to reflect the injected waves multiply in order to achieve isotropic polarization. The properties of microwave transmission and shielding through apertures with different sizes are simulated. The result shows that the coupled E field near the detector region increases with the aperture size whether the aperture lies on the front side or on the reverse side. Fig. 7 gives an example. The minimum coupled electrical field threshold, E_c , is set equivalent to the background noise. The microwave shielding is effective until the aperture size is reduced to below $\lambda/30$. Here, λ is the wavelength. The copper

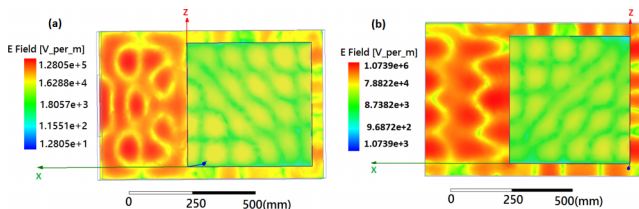


FIG. 7. The coupled E field distribution in the vacuum chamber and detector box with slit of 1 mm × 30 mm. (a) slit in front side; (b) slit in end side.

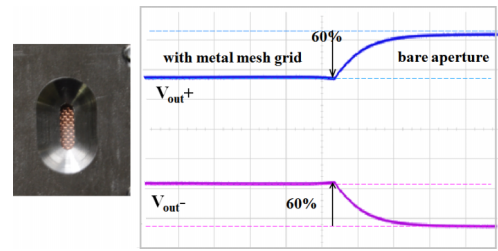


FIG. 8. Light transmission through mesh grid fixed in aperture.

mesh grid in front of the aperture for microwave shielding is analyzed. The spacing g and the wire diameter d of the mesh grid are two critical parameters.¹² In the last EAST experiments, the copper metal mesh with spacing $g \sim 0.635$ mm and wire diameter $d \sim 0.15$ mm was installed in front of the collimating aperture. The optical transmission fraction of the mesh grid is calibrated with visible light, as shown in Fig. 8. The transmission fraction is about 60% which can agree well with the value calculated from the formula in Ref. 12.

V. SUMMARY

The foil resistive bolometer diagnostic on EAST is improved recently for better performance. Part of the detectors were replaced by a new generation of detectors with faster response. Presently, the location of the bolometer detector is very near the RF antenna and the signals suffer a serious influence from RF waves at 2.45 GHz and 4.6 GHz. The microwave interference problem is studied by laboratory tests and simulation. Some shielding methods are employed, but the microwave interference is not resolved completely with the increasing RF wave injection power. The closed circuit inside the detector is a potentially weak component against electromagnetic interference. It is uncertain if it is effective to change the meander layout on the substrate foil or by changing the cable connection inside the detectors. Further work is needed to enhance the anti-interference ability of the detectors and to try and find a way for better microwave shielding.

ACKNOWLEDGMENTS

This work was supported by National Magnetic Confinement Fusion Science Program of China (Grant No. 2015GB103000), Natural Science Foundation of China (Grant Nos. 11305214 and 11575247), and JSPS-NRF-NSFC A3 Foresight Program in the field of Plasma Physics (Grant No. 11261140328).

- ¹R. L. Boivin *et al.*, *Rev. Sci. Instrum.* **70**, 260 (1999).
- ²B. J. Peterson *et al.*, *Plasma Phys. Controlled Fusion* **45**, 1167 (2003).
- ³K. McCormick *et al.*, *Fusion Eng. Des.* **74**, 679 (2005).
- ⁴H. Meister *et al.*, *Rev. Sci. Instrum.* **81**, 10E132 (2010).
- ⁵L. Giannone *et al.*, *Plasma Phys. Controlled Fusion* **47**, 2123 (2005).
- ⁶H. Meister *et al.*, *Rev. Sci. Instrum.* **84**, 123501 (2013).
- ⁷Y. M. Duan *et al.*, *Rev. Sci. Instrum.* **83**, 093501 (2012).
- ⁸K. F. Mast *et al.*, *Rev. Sci. Instrum.* **62**, 744 (1991).
- ⁹Y. M. Duan *et al.*, *Plasma Sci. Technol.* **13**, 546 (2011).
- ¹⁰D. Seo, *Rev. Sci. Instrum.* **81**, 10E128 (2010).
- ¹¹D. Hathiramani *et al.*, *Fusion Eng. Des.* **88**, 1232 (2013).
- ¹²D. Zhang *et al.*, in 38th EPS Conference on Plasma Physics, 2011, P5.056.